Research Article | Vol. 30, No. 23 / 7 Nov 2022 / Optics Express 41350
Optics EXPRESS

Ultrafast modulation of a high harmonic generation in a bulk ZnO single crystal

SHUAI XU,[1,2,3,5] HANG ZHANG,[2,4,5] JUNHONG YU,[2,5] YADONG HAN,[2,4] ZHAN WANG,[1,3,6] AND JIANBO HU[2,4,7]

[1]*Institute of Mechanics, Chinese Academy of Sciences, Beijing, 100190, China*
[2]*Laboratory for Shock Wave and Detonation Physics, Institute of Fluid Physics, China Academy of Engineering Physics, Mianyang 621900, China*
[3]*School of Engineering Science, University of Chinese Academy of Sciences, Beijing 100049, China*
[4]*State Key Laboratory for Environment-Friendly Energy Materials, Southwest University of Science and Technology, Mianyang 621010, China*
[5]*These authors contribute equally*
[6]*zwang@imech.ac.cn*
[7]*jianbo.hu@caep.cn*

Abstract: Optical modulation of high harmonic generation (HHG) is of fundamental interest in science and technology, which can facilitate understanding of HHG generation mechanisms and expand the potential optoelectronic applications. However, the current established works have neither shown the advanced modulation performance nor provided a deep understanding of modulation mechanisms. In this work, taking wurtzite zinc oxide (ZnO) single crystal as a prototype, we have demonstrated an all-optical intensity modulation of high-order HHG with a response time of less than 0.2 ps and a depth of more than 95%, based on the pump-probe configuration with two different pumping wavelengths. Besides the achieved excellent modulation performance, we have also revealed that the modulation dynamics in ZnO single crystal highly depend on the excitation conditions. Specifically, the modulation dynamics with the near-bandgap or above-bandgap excitation are attributed to the non-equilibrium interband carrier relaxations, while for mid-gap excitation, the modulation dynamics are dominated by the nonlinear frequency mixing process. This work may enhance the current understanding of the HHG modulation mechanism and enlighten novel device designs.

1. Introduction

High harmonic generation (HHG) has been discovered in gases and liquids for decades with the development of high-intensity lasers [1,2,3], which have shown various applications in molecular imaging and photoelectronic spectroscopy [4,5]. More recently, the HHG generation in solids (e.g., ZnO [6,7], MgO [8], GaSe [9], MoS_2 [10], SiO_2 [11], graphene [12]) has achieved great success with the lower requirement of driving laser intensity [13]. It has been demonstrated that HHG in solids would be a powerful detection tool for condensed matter physics, showing great application potentials in detecting crystal structure, restructuring the energy band of crystals, and generating attosecond pulses [8,14,15]. Meanwhile, due to its promising prospects in better understanding the HHG generation mechanism and designing novel photonic devices, the all-optical modulation of HHG in solids is becoming frontier research and received enormous research interest.

By far, only a few works about all-optical HHG modulation have been reported: (i) Yang Cheng et al. utilized a pump pulse to modulate HHG in graphene monolayer, and a response time of 60 ps and a modulation depth of 35% are demonstrated [16]; (ii) Zhou Wang et al. modulated HHG in ZnO via photo-carrier doping, which shows that the response time could be hundreds of picoseconds and the modulation depth could be larger than 90% [17]; (iii) Bionta. M. R. et

#462638 https://doi.org/10.1364/OE.462638
Journal © 2022 Received 29 Apr 2022; revised 21 Jul 2022; accepted 3 Aug 2022; published 26 Oct 2022

Optics EXPRESS

al. modulated HHG in VO_2 via photo-induced phase transition, showing a response time of tens of picoseconds and a modulation depth of larger than 90% [18]; (iv) Christian Heide et al modulated the HHG in MoS_2 via resonant photodoping with a modulation depth of 50% [19]. All the modulations were based on above-bandgap and linear excitation. Therefore, the modulation parameters have only been explored very limitedly. On the other side, the reported works have not shown good modulation performance (e.g., the response time is tens of picoseconds or even longer).

In this work, using ZnO single crystal as a prototype, we demonstrate the all-optical modulation of the HHG at various excitation conditions to better understand the modulation mechanism. We have revealed two distinct modulation mechanisms, depending on the excitation parameters. For near-bandgap or above-bandgap excitation conditions, the modulation is due to the recombination processes from quasi-continuum broad defect states and the conduction band to the valence band, while for mid-gap excitation, the modulation results from both mixing-frequency spots radiation and the interband recombination. Moreover, an excellent modulation performance has been demonstrated, in which the intensity of HHG is decreased to less than 5% of initial, showing a modulation depth of more than 95%, and the ultrafast response time, determined by the descending edge and the rising edge of HHG dynamics, is demonstrated to be less than 0.2 ps.

2. Results and discussion

As shown in Fig. 1(a), a regenerative amplified Ti: sapphire system (Spectra-Physics), emitted femtosecond laser pulses with a central wavelength of 800 nm, the pulse duration of 50 fs, and the repetition rate of 1 kHz, has been used as the laser source. A TOPAS laser system, converting the 800 nm pulse to the middle-infrared (MIR) beam of 2350 nm, has been used to generate the HHG in a (0001)-cut ZnO single crystal with a thickness of 0.5 mm. To obtain relatively strong and stable HHG signals, we have fixed the fluence of the MIR beam at 400 mJ/cm^2, under which condition no physical damage in the ZnO crystal has been observed. Figure 1(b) shows the spectra of the HHG signals with the fifth (HH5) to the ninth (HH9) order driven by the MIR beam. Due to the lattice symmetry of (0001)-cut ZnO single crystal, only odd-order HHG signals could be detected. This phenomenon is rational and was observed in several other works [6,7]. Another 800 nm pulse emitted from the femtosecond laser source could be frequency-doubled by a BBO crystal to serve as the pump beam, which has been used to modulate the HHG and then focused on the ZnO crystal at the same position as the MIR beam. The intensity of the pump beam has been controlled by the combination of a half-wave plate and a polarizer. A time-delay device, synchronized to the spectrometer by a computer, has been used to adjust the time separation between the pump and MIR beams. The HHG spectra, modulated by the pump as a function of the time separation, are shown in Figs. 1(c) and 1(d) for the 400 nm and 800 nm pump wavelength, respectively. It is demonstrated that when the delay is positive (i.e., the pump pulse arrives earlier than the MIR probe pulse), the intensity can be suppressed for all orders of HHG.

More detailed HHG dynamic results are shown in Fig. 2, in which Fig. 2(a) is 400 nm pumping and Fig. 2(b) is 800 nm pumping that the pump fluence is 13mJ/cm^2. All orders of HHG have shown similar behaviors: the pump light can suppress HHG when the delay is positive, followed by a recovery process. The recovery dynamics consist of two sub-processes: a fast process whose time scale is picosecond and a slow process which is almost a platform in our measured time window. By exponentially fitting the experimental data, we have determined that the time constant of the fast process is 3.4 ps for the 400 nm excitation and 0.15 ps for the 800 nm excitation, respectively.

In contrast, the pump-probe experiment of (0001)-cut ZnO has also been done by selecting the pump wavelength of 400 nm (Fig. 2(c)) or 800 nm (Fig. 2(d)) and the probe wavelength of 470 nm (the wavelength of HH5) with the pump fluence of 5mJ/cm^2. The time constant of the fitted

Optics EXPRESS

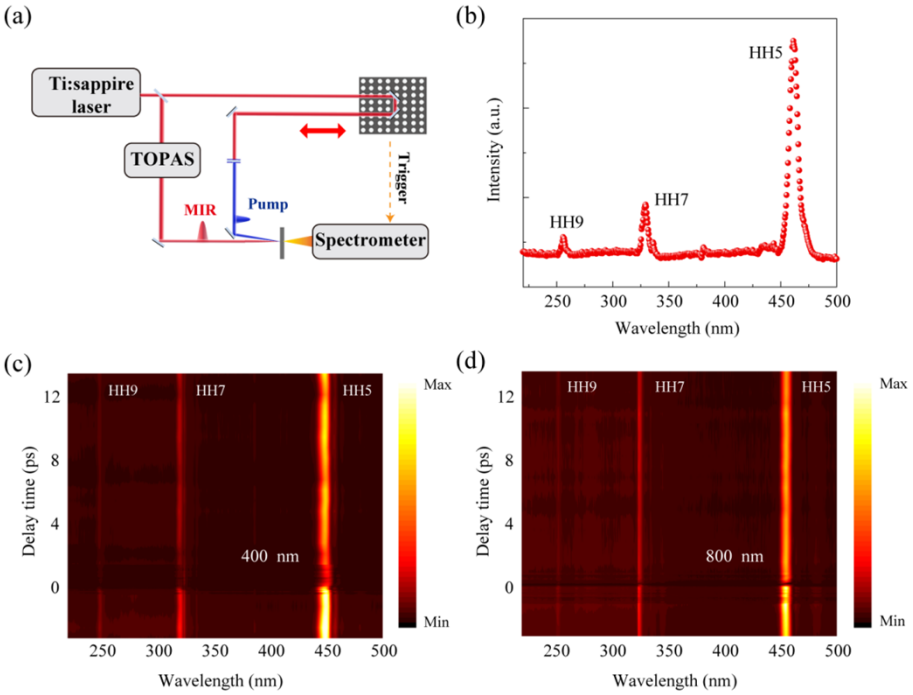

Fig. 1. (a) The sketch map of the experimental setup. (b) HHG spectra driven by a MIR femtosecond laser of 2350 nm in a (0001)-cut ZnO single crystal. The HHG spectra as a function of delay at the condition of (c) 400 nm pump and (d) 800 nm pump.

curve is 2.6 ps in Fig. 2(c) and 0.18 ps in Fig. 2(d), which is the same order of magnitude as the fast process in Figs. 2(a) and 2(b). Good agreements between the two experiments indicate that the process of HHG modulation dynamics can reflect the excitation and relaxation processes of electrons, which may enlighten the mechanism of HHG modulation. More discussions will be given later.

The pump fluence-dependent experiments have been done to understand further the distinct modulation dynamics with different excitation wavelengths, shown in Figs. 3(a) and 3(b). In this experiment, an excellent performance of HHG modulation has been demonstrated. At the lowest point, the intensity of HHG could be less than 5% of the initial, which means the modulation depth could be more than 95%. The response time, which depends on the descending edge and the rising edge of HHG, could be less than 0.2 ps when the pump wavelength is 800 nm. The large modulation depth and the ultrafast response time show considerable potential in the future.

Besides the excellent modulation performance, we have also concluded that the slow process would be more evident when the pump fluence becomes higher while the fast process is contrary. For the 400 nm excitation, the fast process could seldom be observed when the pump fluence is higher than 13 mJ/cm^2. For the 800 nm excitation, similar fluence-dependent behavior has been observed. At 7 mJ/cm^2, the fast process has dominated the whole recovery process with almost no slow process. The weight of the fast process is 75% at 13 mJ/cm^2, while at 115 mJ/cm^2, it is only 30%.

To identify the carrier excitation processes in our experiments, we measured the changes in relative intensities of HH5 at the zero delay versus pump fluences, as shown in Fig. 3(c). When the pump fluence is low, the relative intensities of HHG change rapidly as the pump fluence changes. While for high pump fluence, the relative intensities have almost no dependence on the

Optics EXPRESS

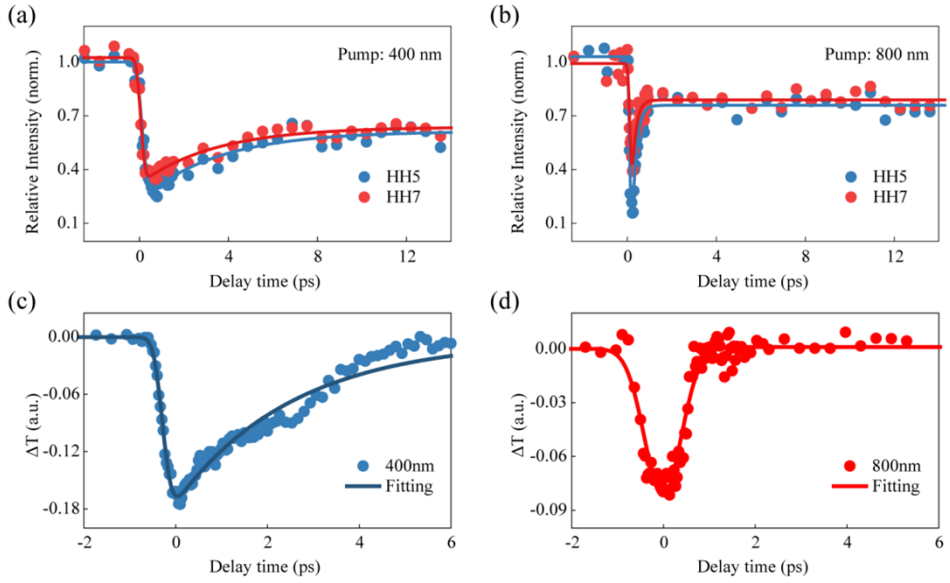

Fig. 2. The results of HHG modulation experiments and pump-probe experiments. Dots are data and lines are the fitted curve of the data. (a) shows the relative intensities of HH5 and HH7 versus delay when the pump wavelength is 400 nm. (b) shows the relative intensities of HH5 and HH7 versus delay when the pump wavelength is 800 nm. (c) and (d) show the pump-probe experimental results when the probe is 470nm, where (c) is 400 nm excitation and (d) is 800 nm excitation, respectively. The ylable of (c) and (d) is the change of the transmissivity in the normal pump-probe experiment.

pump intensity since the inhibition effect of HHG is saturated. Thus we have fitted the curves at the low pump region via the power-law fitting. For 400 nm excitation, the scaling factor is 1.75, indicating the mixed excitations: the electrons would be excited to the conduction band via two-photon absorption or to a state below the conduction band via one-photon absorption (the band gap of ZnO is 3.37 eV). For 800 nm excitation, the scaling factor is 1.04, indicating that one-photon absorption dominates the excitation process. It means that the fast process under the 800 nm excitation could not be the relaxation processes of electrons in the conduction band since one photon's energy is less than the bandgap of ZnO. Beyond the low-fluence region, the above-bandgap excitation would dominate the excitation process via multi-photon absorption.

Based on the above results, the modulation dynamics in HHG can be interpreted via the carrier dynamics, which show two distinct modulation mechanisms highly depending on the pumping wavelength. For the 400 nm excitation, the carrier dynamics in Fig. 2(c) have been discussed in our previous work [20], enlightening the HHG modulation mechanism. For the near-bandgap excitation, one electron could be excited to the quasi-continuum broad defect states in the bandgap via absorbing one photon of 400 nm, whose recombination time at the valence band is 2.5ps [20]. This has been considered the origin of the fast process in Fig. 2(a). For the above-bandgap excitation via two-photon absorption, one electron could be excited to the conduction band; thus, the slow process should be attributed to the interband recombination, whose time constant is hundreds of picoseconds [21].

On the other hand, how the carrier dynamics affect the intensity of HHG could be further understood based on the well-known three-step model for HHG generation, that is, (i) electron tunneling excitation, (ii) electron or hole acceleration, and (iii) electron-hole recombination [22,24–27]. Based on this model, the contribution of HHG could be divided into two types:

Optics EXPRESS

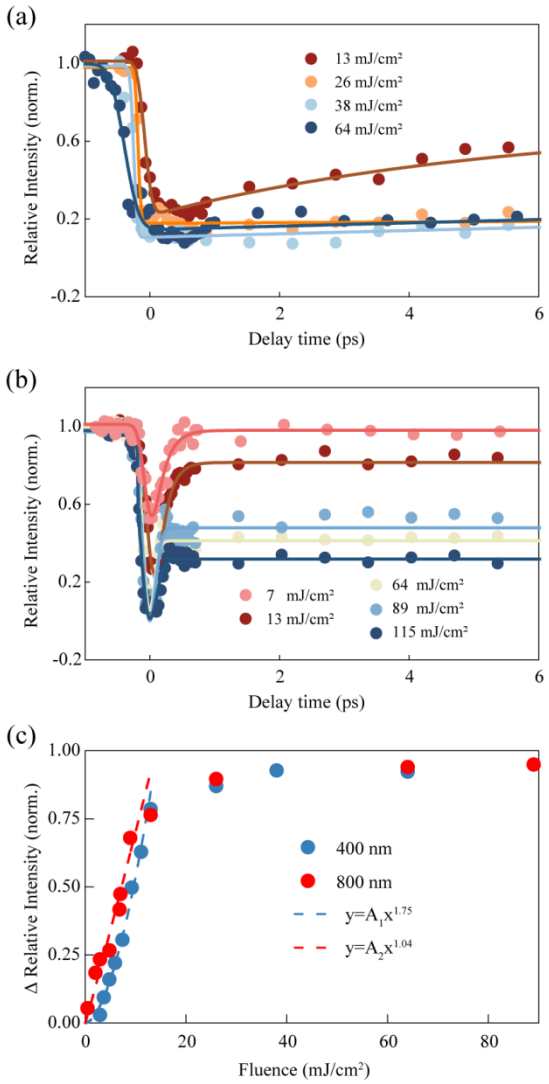

Fig. 3. (a) The relative intensities of HH5 versus delay with different pump fluences for 400 nm excitation. The points are experimental data and the lines are the fitted curves. (b) The relative intensities of HH5 versus delay with different pump fluences for 800 nm excitation. The points are experimental data and the lines are the fitted curves. (c) The change of relative intensities of HH5 at the zero delay at different pump fluences. The ylable means the change of the relative intensity from initial to the zero delay in the pump-probe HHG experiment. The equation of the fitted curves is $y = Ax^q$. The parameter q is 1.04 for 800 nm excitation and 1.75 for 400 nm excitation.

Optics EXPRESS

intraband HHG and interband HHG, which are generated by the second and the third step of the three-step model, respectively. With a pre-excitation pump, the population of carriers would be changed both in the valence band and conduction band. The excited carriers would suppress the intensity of HHG because it might, to a large extent, inhibit the interband HHG, which is the dominant HHG contribution in ZnO [17]. This should be caused by the strong scattering effect, which could prolong the electron-hole dephasing rate and suppress the interband HHG [19]. After the zero delay, the relaxation of the electrons will diminish the inhibition effect of HHG, shown as the recovery process in our experiment. Thus it is rational that the HHG modulation experiments can reflect the carrier dynamics of ZnO. Meanwhile, the fluence-dependent experiments can also be explained. With low pump fluence, partial electrons are excited to the quasi-continuum broad defect states via one-photon absorption. Others are excited to the conduction band via two-photon absorption. Thus, both fast and slow processes have been observed. While at high pump fluences, most electrons are excited to the conduction band that the slow process would dominate the recovery process. In this case, the pump fluence should have almost no effect on the modulation depth (Fig. 3(c)) that the inhibition effect is saturated. A large population of excited electrons suppresses the interband HHG to zero and only intraband HHG with weak intensity remains.

It is worth noting that several sub-processes originating from carrier decay among discrete defect states have been observed in Fig. 2(c), which were already discussed in detail in ref. [20]. While in Fig. 2(a), they are seldom observed, which should show the difference between the HHG modulation experiment and the pump-probe experiment. This is rational according to the three-step model of HHG [22], which means that HHG is dependent on the carriers in the conduction band and valence band. Thus, the HHG modulation experiment would be more sensitive to detecting the recombination process at the valence band than seeing carrier decay among discrete defect states.

For the 800 nm excitation, one-photon absorption could only excite one electron to a virtual mid-gap state, which could be further supported in the following emission experiment, showing another different modulation mechanism from the near-bandgap or above-bandgap excitation. As shown in the inset of Fig. 4(a), several emission spots have been observed when the delay is near zero in the HHG modulation experiments. The emission angles of the spots are different from that of MIR or pump. In principle, five emission spots can be generated due to the frequency mixing: an orange spot (597 nm, $\omega_{pump} + \omega_{MIR}$), a blue spot (472 nm, $\omega_{pump} + 2\omega_{MIR}$), a purple spot (337 nm, $\omega_{pump} + 4\omega_{MIR}$), an ultraviolet spot (295 nm, $\omega_{pump} + 5\omega_{MIR}$), and a green spot ($2\omega_{pump}$ - ω_{MIR}). Four of them have been detected in our experiment. The 393 nm ($\omega_{pump} + 3\omega_{MIR}$) spot near the bandgap has not been observed, considered to be reabsorbed by ZnO. These spots are thought to arise from the nonlinear frequency mixing process between the MIR pulse and the pump pulse, as observed before in Ref. [23].

The intensity dynamics of the blue and purple spots have also been investigated, shown in Fig. 4(a). Comparing the HHG dynamics in Fig. 2(b) with the spots' dynamics, the processes coincide well near the zero-time delays (-0.5 ps~0.75 ps), further indicating the fast process for 800 nm excitation should have relationships with the spots. More importantly, the blue spot with the most significant intensity, originating from the frequency mixing between one pump photon and two MIR photons, is another piece of evidence to support our explanation: one 800 nm photon could excite one electron at a mid-gap state whose lifetime is quite small. When the pump and MIR pulses are overlapped, it would suppress HHG and radiate mixing-frequency spots.

Thus the mechanism of the fast process for 800 nm excitation could be interpreted as the mixing-frequency spots radiation. Near the region of zero delays, when the pump and MIR pulses are overlapped, electrons are pumped to a virtual mid-gap state and then driven by several MIR photons. We have conjectured that the energy of MIR would be consumed to radiate the mixing-frequency spots; thus, the HHG would be suppressed. Based on this, it is rational that the

Optics EXPRESS

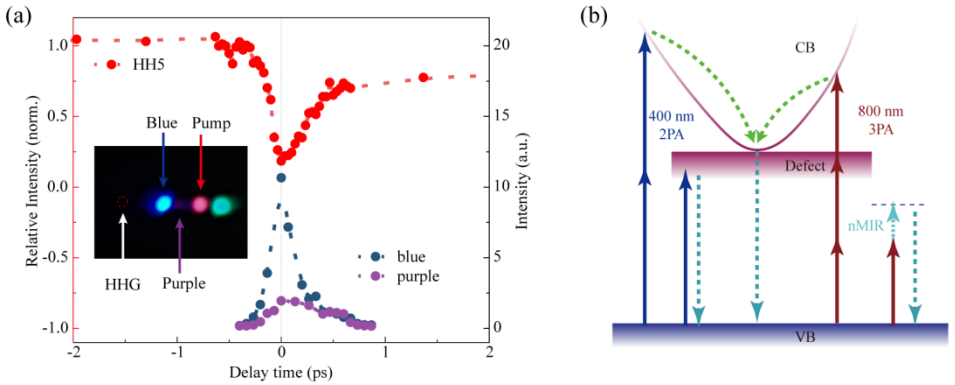

Fig. 4. (a) The intensities of blue spot and purple spot versus delay compared with the relative intensity of HH5. The inset is the picture of mixing-frequency spots. The positions of HHG, pump light, blue spot, and purple spot are labeled. (b) The sketch map of the mechansims.

energy of HHG would be the lowest while the mixing-frequency spots are contrary when the delay is zero in Fig. 4(a). Also, the lifetime of the fast process within hundreds of femtoseconds could be interpreted for it would vanish when the pump and MIR pulses completely separate. A much slower process has been observed at larger pump intensities, which should be attributed to interband recombination that partial electrons are excited to the conduction band via three-photon absorption [21].

Finally, a schematic of the modulation mechansims has been shown in Fig. 4(b). In this figure, the upward arrows indicate the excitation process while the downward arrows indicate the recombination process. The left half of the figure is the 400 nm pumping condition with two excitation processes. One-photon process could excite the electrons from VB to the quasi-continuum broad defect state while two-photon process could excite the electrons from VB to CB. The right half is the 800 nm pumping condition that contains the mixing-frequency radiation process. With high pump fluence, the electrons could also be excited from VB to CB via three-photon absorption.

3. Conclusion

In conclusion, the optical modulation of HHG generated in (0001)-cut wurtzite ZnO bulk crystal has been demonstrated with different pumping wavelengths. An excellent modulation performance has been achieved with all orders of HHG being ultrafast and effectively suppressed. According to our experimental results, the ultrafast response time could be less than 0.2 ps, and the modulation depth could be more than 95%. Furthermore, we have revealed that two different modulation mechanisms would dominate the HHG modulation dynamics, highly depending on the pumping wavelength. For the 400 nm excitation, the fast recovery process with a lifetime of 3.4 ps is considered as the recombination process from quasi-continuum broad defect states to the valence band; however, the slow recovery process is the interband recombination process. While for the 800 nm excitation, extremely high-speed dynamics occurring on the time scale of 0.15 ps are identified, which can be attributed to the mixing-frequency spots radiation. This work has provided an effective and convenient way to modulate HHG in solids with excellent performances. We expect that HHG would have better performance in ultrafast science and semiconductor physics.

Optics EXPRESS

Funding. Science Challenge Project (No. TZ2018001); Project of State Key Laboratory of Environment-friendly Energy Materials, Southwest University of Science and Technology (No. 21fksy07); National Natural Science Foundation of China (No. 11872058).

Disclosures. The authors declare no conflicts of interest.

Data availability. Data underlying the results presented in this paper are not publicly available at this time, but may be obtained from the authors upon reasonable request.

References

1. M. Ferray, A. L'Huillier, X. F. Li, L. A. Lompre, G. Mainfray, and C. Manus, "Multiple-harmonic conversion of 1064 nm radiation in rare gases," J. Phys. B-At. Mol. Opt. **21**(3), L31–L35 (1988).
2. T. T. Luu, Z. Yin, A. Jain, T. Gaumnitz, Y. Pertot, J. Ma, and H. J. Worner, "Extreme-ultraviolet high-harmonic generation in liquids," Nat. Commun. **9**(1), 3723 (2018).
3. A. Flettner, T. Pfeifer, D. Walter, C. Winterfeldt, C. Spielmann, and G. Gerber, "High-harmonic generation and plasma radiation from water microdroplets," Appl. Phys. B. **77**(8), 747–751 (2003).
4. A. Baltuska, T. H. Udem, M. Uiberacker, M. Hentschel, E. Goulielmakis, C. H. Gohle, R. Holzwarth, V. S. Yakovlev, A. Scrinzi, T. W. Hansch, and F. Krausz, "Attosecond control of electronic processes by intense laser fields," Nature **421**(6923), 611–615 (2003).
5. J. Itatani, J. Levesque, D. Zeidler, H. Niikura, H. Pepin, J. C. Kieffer, P. B. Corkum, and D. M. Villeneuve, "Tomographic imaging of molecular orbitals," Nature **432**(7019), 867–871 (2004).
6. S. Ghimire, A. D. DiChiara, E. Sistrunk, P. Agostini, L. F. DiMauro, and D. A. Reis, "Observation of high-order harmonic generation in a bulk crystal," Nat. Phys. **7**(2), 138–141 (2011).
7. S. Gholam-Mirzaei, J. Beetar, and M. Chini, "High harmonic generation in ZnO with a high-power mid-IR OPA," Appl. Phys. Lett. **110**(6), 061101 (2017).
8. Y. S. You, D. A. Reis, and S. Ghimire, "Anisotropic high-harmonic generation in bulk crystals," Nat. Phys. **13**(4), 345–349 (2017).
9. O. Schubert, M. Hohenleutner, F. Langer, B. Urbanek, C. Lange, U. Huttner, D. Golde, T. Meier, M. Kira, S. W. Koch, and R. Huber, "Sub-cycle control of terahertz high-harmonic generation by dynamical Bloch oscillations," Nat. Photonics **8**(2), 119–123 (2014).
10. H. Z. Liu, Y. L. Li, Y. S. You, S. Ghimire, T. F. Heinz, and D.A. Reis, "High-harmonic generation from an atomically thin semiconductor," Nat. Phys. **13**(3), 262–265 (2017).
11. T. T. Luu, M. Garg, S. Y. Kruchinin, A. Moulet, M. T. Hassan, and E. Goulielmakis, "Extreme ultraviolet high-harmonic spectroscopy of solids," Nature **521**(7553), 498–502 (2015).
12. N. Yoshikawa, T. Tamaya, and K. Tanaka, "High-harmonic generation in graphene enhanced by elliptically polarized light excitation," Science **356**(6339), 736–738 (2017).
13. S. C. Jiang, J. G. Chen, H. Wei, C. Yu, R. F. Lu, and C. D. Lin, "Role of the transition dipole amplitude and phase on the generation of odd and even high-order harmonics in crystals," Phys. Rev. Lett. **120**(25), 253201 (2018).
14. G. Vampa, T. J. Hammond, N. Thire, B. E. Schmidt, F. Legare, C. R. McDonald, T. Brabec, D. D. Klug, and P. B. Corkum, "All-optical reconstruction of crystal band structure," Phys. Rev. Lett. **115**(19), 193603 (2015).
15. A. A. Lanin, E. A. Stepanov, A. B. Fedotov, and A. M. Zheltikov, "Mapping the electron band structure by intraband high-harmonic generation in solids," Optica **4**(5), 516–519 (2017).
16. Y. Cheng, H. Hong, H. Zhao, C. C. Wu, Y. Pan, C. Liu, Y. G. Zuo, Z. H. Zhang, J. Xie, J. H. Wang, D. P. Yu, Y. Ye, S. Meng, and K. H. Liu, "Ultrafast optical modulation of harmonic generation in two-dimensional materials," Nano. Lett. **20**(11), 8053–8058 (2020).
17. Z. Wang, H. Park, Y. H. Lai, J. L. Xu, C. I. Blaga, F. Y. Yang, P. Agostini, and L. F. DiMauro, "The roles of photo-carrier doping and driving wavelength in high harmonic generation from a semiconductor," Nat. Commun. **8**(1), 1686 (2017).
18. M. R. Bionta, E. Haddad, A. Leblanc, V. Gruson, P. Lassonde, H. Ibrahim, J. Chaillou, N. Emond, M. R. Otto, A. Jimenez-Galan, R. E. F. Silva, M. Ivanov, B. J. Siwick, M. Chaker, and F. Legare, "Tracking ultrafast solid-state dynamics using high harmonic spectroscopy," Phys. Rev. Res. **3**(2), 023250 (2021).
19. C. Heide, Y. Kobayashi, A. C. Johnson, F. Liu, T. F. Heinz, D. A. Reis, and S. Ghimire, "Probing electron-hole coherence in strongly driven 2D materials using high-harmonic generation," Optica. **9**(5), 512–516 (2022).
20. C. Gu, H. Zhang, Y. G. Liu, J. H. Yu, J. H. Pan, G. Q. Luo, Q. Shen, J. Tang, and J. B. Hu, "Time-domain observation of spectral diffusion in defective ZnO," ACS Omega. **6**(23), 15442–15447 (2021).
21. G. Wang, S. Xiao, Y. H. Peng, Y. W. Wang, C. L. Yuan, and J. He, "Two-photon and three-photon absorption in ZnO nanocrystals embedded in Al_2O_3 matrix influenced by defect states," Opt. Lett. **44**(1), 179–182 (2019).
22. C. Yu, S. C. Jiang, and R. F. Lu, "High order harmonic generation in solids: a review on recent numerical methods," Adv. Phys-X **4**(1), 1562982 (2019).
23. P. Jurgens, B. Liewehr, B. Kruse, C. Peltz, and A. Mermillod-Blondin, "Origin of strong-field-induced low-order harmonic generation in amorphous quartz," Nat. Phys. **16**(10), 1035–1039 (2020).
24. G. Vampa, C.R. McDonald, G. Orlando, D. D. Klug, P. B. Corkum, and T. Brabec, "Theoretical analysis of high-harmonic generation in solids," Phys. Rev. Lett. **113**(7), 073901 (2014).

Optics EXPRESS

25. E. N. Osika, A. Chacon, L. Ortmann, N. Suarez, J. A. Perez-Hernandez, B. Szafran, M. F. Clappina, F. Sols, A. S. Landsman, and M. Lewenstein, "Wannier-Bloch approach to localization in high-harmonic generation in solids," Phys. Rev. X. **7**, 021017 (2017).
26. L. Yue and M. B. Gaarde, "Imperfect recollisions in high-harmonic generation in solids," Phys. Rev. Lett. **124**(15), 153204 (2020).
27. M. Lewenstein, Ph. Balcou, M. Yu. Ivanov, Anne L'Huillier, and P. B. Corkum, "Theory of high-harmonic generation by low-frequency laser fields," Phys. Rev. A. **49**(3), 2117–2132 (1994).